Published by :
http://www.ijert.org

International Journal of Engineering Research & Technology (IJERT)
ISSN: 2278-0181
Vol. 10 Issue 09, September-2021

Influence of Gd^{+3} Cation Substitution on the Functional Properties of $Al_{0.8}La_{0.2}TiO_3$ Nanoparticles

S Dastagiri[1*], V. Ramesh Kumar[2], K. E. Supriya[1], M. V. Saritha[1], M. Rajamohan Rao[1] and M. V. Lakshmaiah[1**]
[1]Department of Physics, Sri Krishnadevaraya University, Ananthapuramu, A.P, India-515003
[2]Department of Physics, Government Degree College, Atmakur, Kurnool, A.P, India-518003

Abstract:- **In present, the work reports on the effect of Gd-substitution on Aluminum Lanthanum Titanate (ALT) perovskite structures, structural and optical properties. The $Al_{0.8}Gd_yLa_{0.2-y}TiO_3$ (y= 0.01, 0.02, 0.03, 0.04) (AGLTO) hydrothermally synthesized nanoparticles. The XRD indicates crystallite size, Micro-strain, dislocation density and FWHM (full-width half maxima). The Scherer's formula and Williamson-Hall (W-H) analysis used the X-ray peak expansion technique to determine the crystalline sizes and lattice strain; it was observed that an inversely proportional relationship exists. Fourier transforms infrared spectra (FT-IR) tested the presence of Al-O, Gd-O, La-O & Ti-O based metal oxide (M-O) bonds at A & B sites. The E_g values are increased from 3.293 to 3.372 eV with increase of Gd content from y = 0.01 to 0.04 contents show the wide E_g values suggesting optoelectronic and sensor applications.**

1. INTRODUCTION

The perovskite titanates doped with rare earth components offered fascinating structural, morphological, electrical, dielectric, magnetic, magneto-caloric and piezoelectric, etc., properties [1]. Numerous researchers focused on different properties of notable perovskite titanates like MTiO3 (M = Ba, Ni, Mg, Sr, Pb, Al, La, Ca, Zn, Mn, Co, Eu, Zr and so forth,) [1]. Among these titanates, the aluminum titanates (AT) were concentrated in an exceptionally restricted way. Aluminum titanate perovskites were concentrated by past researchers [2-6] for primary, optical, photocatalytic, electrical and mechanical properties.

Specifically, Sahu et al. [2], arranged the AT nanoparticles and detailed the tetragonal design and dielectric properties. Azarniya et al. [3], fostered the AT nanoparticles just as nanofibers. Further, the inside and out microstructure was explored. Bakhshandeh et al [4], detailed he photocatalytic action of AT nanoparticles. Ewais et al. [5], separated the AT based earthenware production from the aluminum sludge waste. Tang et al. [6], noticed the goliath electro rheological impacts in AT nanoparticles. From this review, unmistakably the writing on AT and its based nanomaterials was not accessible in a bountiful way. To expand the dielectric steady of $Al_{0.8}La_{0.2}TiO_3$, we wanted to substitute the Gd-rare earth component. Consequently, the $Al_{0.8}Gd_yLa_{0.2-y}TiO_3$ (y = 0.01 - 0.04)/AGLTO nanoparticles were arranged through aqueous strategy, wherein a few benefits like low working temperatures, less force and tedious, great crystallinity, simple example planning, and modest were accomplished [7].

2. EXPERIMENTAL PART

To set up the AGLTO nanoparticles, the trailblazer materials like La $(NO_3)_3.6H_2O$ (99.8% temperance, Sigma-Aldrich), Al $(NO_3)_3$ $9H_2O$ (99.8% flawlessness, Sigma-Aldrich), $Gd(NO_3)_3$. $6H_2O$ (99.9% faultlessness, Sigma-Aldrich), and TiO_2 (99.9% temperance, Sigma-Aldrich) were taken into another glass container containing refined water as per the stoichiometric extent. With the help of appealing stirrer, the forerunner mix was blended at a consistent blending speed of 420 rpm. After some time, the white and blended nitrate game plan was outlined. Finally, they got course of action was moved to another Teflon bowl of 300 ml limit. Thusly, the Teflon bowl containing the game plan was brought into the solidified steel autoclave. By then, to play out the watery reaction, the autoclave was kept inside the hot air oven for 8 h at 150ºC. Besides, the autoclave was chilled off to room temperature followed by the ejection of tests from the Teflon bowl. Accordingly, they got test was cleaned for a couple of times until the pH worth of the model shows up at 7. In addition, using the hot air grill, the model was dried for 120 min at 60º C. Fittingly, they got AGLTO nanoparticles gone through different depictions, for instance, X-ray diffractometer (XRD, Bruker, CuKa, k = 0.15406 nm), FT-IR spectrophotometer (IR inclination 1, Shimadzu) and UV–Apparent spectrophotometer (JASCO, V-670 PC) to ponder the underlying and optical properties, separately.

3. XRD ANALYSIS

The X-ray diffraction patterns of AGLTO nanoparticles are recording as shown in Fig.1. These patterns provided multiple number of diffraction peaks indicating the polycrystalline nature. It is observed that the maximum intensity is recorded at two-theta angle 13.472º for all the samples. From the maximum intensity (I_{max}) data (see Table.1), it's find that the intensity of the maximum peak position is increased from 6155 to 11840 with increase of Gd-content in the $Al_{0.8}La_{0.2}TiO_3$ system. Therefore, it is confirmed that the substitution of Gd-element induced the crystallinity of $Al_{0.8}La_{0.2}TiO_3$. However, its notice that these peak positions are not matched with any standard structure. Herein, the peak positions of x = 0.01 – 0.04 contents are identifying to be

International Journal of Engineering Research & Technology (IJERT)
ISSN: 2278-0181
Vol. 10 Issue 09, September-2021

similar. Therefore, it indexed this unknown structure as X-structure. Furthermore, the average crystallite size (D) is evaluated using the Scherrer equation: $D = 0.9\lambda/\beta Cos\theta$, λ = wavelength of the CuKα spectral line (0.15406 nm), β = full width half maxima (FWHM) and θ = angle of diffraction [8]. The achieved data ensured that the D is note down to be altering from 23.2 to 41.5 nm for x = 0.01 – 0.04. The disorganized distinction trend is observed due to the unsystematic FWHM values. As the Gd^{+3} cations are substituted into the $Al_{0.8}La_{0.2}TiO_3$ system, the resultant X-structure will be contracted. The reason can be well understood by Shannon ionic radii table [9]. According to this table, the ionic radii of cations are give as, Al^{+3}: 0.039 nm, La^{+3}: 1.22 Å, Gd^{+3}: 1.053 Å, and Ti^{+4}: 0.68 Å. In the AGLT resultant structure, the Gd^{+3} cations of small ionic radii can replace the La^{+3} cations of high ionic radii. Thus, the dimensions of the building block will be decreased. These result can be attributed to the significant homogeneity of the prepared AGLTO nanoparticles shown in Table.1; where dislocation density (ρ) shows the values between 5.806 x 10^{14} and 18.57 x 10^{14} m^{-2} respectively; an alternative form of the Gd contents is y = 0.01 to 0.04.This trend is attributed to the molecular weight of the sample is that raise from 145.412 to 145.963 g/mol as a content with "y".

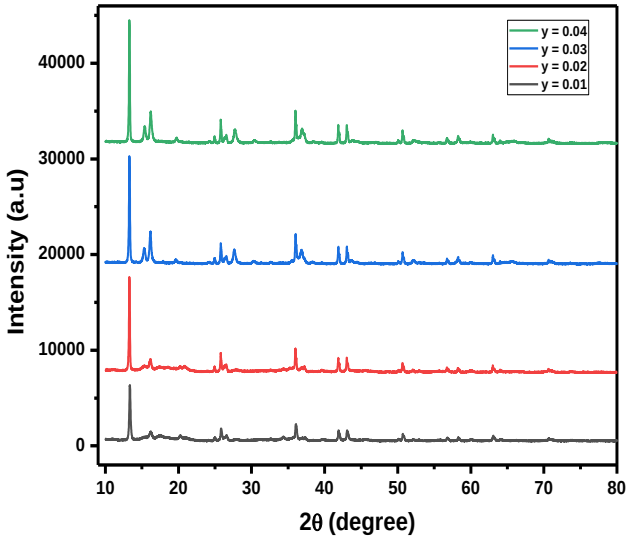

Fig.1. XRD spectra of AGLTO nanoparticles

Table: 1. Data on structural and physical parameters of AGLTO nanoparticles

y	0.01	0.02	0.03	0.04
D (nm)	23.2	41.5	38	37.9
I_{max}	6155	9185	10421	11840
M (g/mole)	145.412	145.596	145.779	145.963
FWHM (β) (radian)	0.9676	0.4031	0.4437	0.4592
ε	0.00457	0.00337	0.00330	0.00478
ε'	0.00124	0.00123	0.00107	0.00272
D'	26.4	45.6	38.4	38.3
ρ (m^{-2})	18.579 x 10^{14}	5.806 x 10^{14}	6.925 x 10^{14}	6.961 x 10^{14}

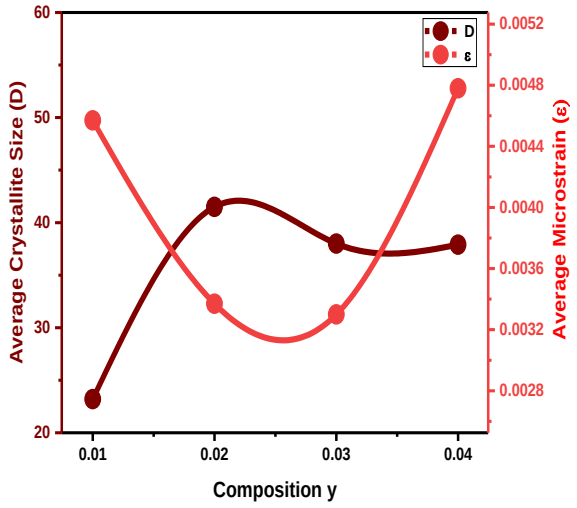

Fig.2. Compositional dependence of D & ε of AGLTO nanoparticles

Williamson - Hall (W - H) plot (Fig.3) is a known planning tool for estimating the average size of crystals (D′) and fine deformation. W-H schemas are developed between βCosθ versus 4Sinθ of the current study using compatible linear relationships:

$$\beta Cos\theta = \frac{0.9\lambda}{D'} + \varepsilon' 4\sin\theta \text{ (i .e. } y = c + mx \text{ form)},$$

Here, the slope of the straight line is related to microstrain (ε'), and the intercept value is related to the crystallite size (D'). The resulting values ε' and D' are listed in Table 1. Finally, a good agreement is noticed between the values derived from the W - H plots based on Scherrer's theory and the values ε' & D'. Based on the formula x = 0.01 to 0.02, D' increases and x = 0.03 -0.04 decreases D'. Micro-strain (ε') is decreases from x = 0.01 - 0.03 after x= 0.04 increase ε' [11]. It can be seen in Fig.2, that there is an inverse proportional relationship between the two parameters D & ε [10]. In literature, similar types of results have been published. [9-12].

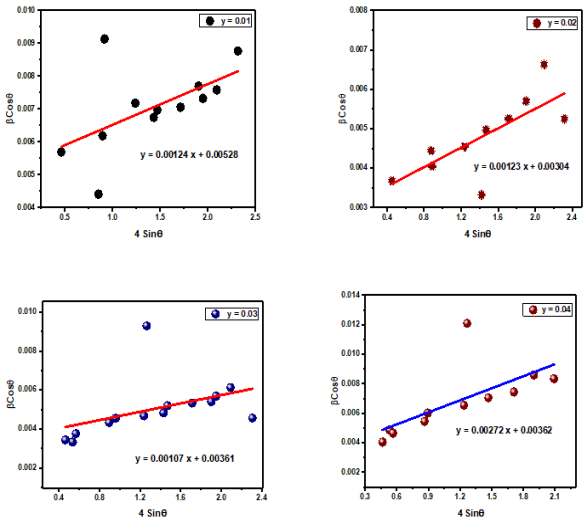

Fig.3. W-H Plots of AGLTO nanoparticles

International Journal of Engineering Research & Technology (IJERT)
ISSN: 2278-0181
Vol. 10 Issue 09, September-2021

4. UV-VIS ANALYSIS

In order to calculate the optical energy gap (E_g), the Kubelka-Munk function is consider. Using this, the function of reflectance F(R): $(1-R)^2/2R$, (where R = reflectance which is recorded from diffuse reflectance spectra as shown in the inset of Fig.4 is computed [13]. Herein, the F(R) is observed to be directly proportional to the absorptivity (α) and therefore, in place of 'α', its can substitute F(R). Further, using the equation: $(\alpha h\nu)^n = m (h\nu - E_g)$ and the $(\alpha h\upsilon)^n$ versus photon energy (hυ) plots, it is calculating the E_g values of AGLT. The exponent (n) in the band gap equation is taken as 2 for direct transition of charge carriers between two energy bands [13]. The $(\alpha h\upsilon)^n$ versus hυ plots of x = 0.01-0.04 contents showed the linear portions. These linear portions are extrapolated towards the hυ-axis. Then, using the intersecting position of the straight line at the hυ-axis, wherein α approaches to zero, the E_g values are calculated. These E_g values are indexed in Fig.4. The results indicates that the E_g values are increased from 3.293 to 3.372 eV with increase of Gd-content from x = 0.01 to 0.04. This kind of behavior is mainly attributed to the oxygen vacancies present in the each composition. That is, the E_g value will be high for the less number of oxygen vacancy and vice versa [13]. In case of AGLT nanoflowers, the numbers of oxygen vacancy are decreased with increase f Gd-content. Therefore, the concerned distances between the valence and conduction bands are increased from 3.293 to 3.372 eV (see Table 2). However, the x = 0.01-0.04 contents show the wide E_g values suggesting optoelectronic and sensor applications [13].

Table.2. Optical band gap (E_g) of AGLTO nanoparticles

y	0.01	0.02	0.03	0.0.4
Optical band gap (E_g) eV	**3.293**	**3.303**	**3.338**	**3.372**

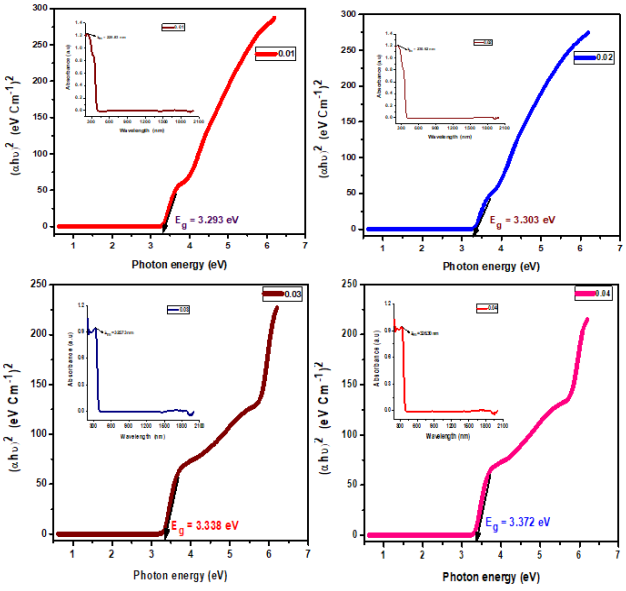

Fig.4. $(\alpha h\upsilon)^2$ versus hυ plots of AGLTO nanoparticles

5. FT-IR ANALYSIS

The Fourier transform infrared spectra (FTIR) spectra of AGLT nanoparticles are recorded over 4000 - 400 cm^{-1} wave number range and show in Fig.5. The A and B-site locations are indexed using the ν_a and ν_b. These two positions suggest indirectly the formation of perovskite structure. The ν_a and ν_b peaks are notice during the range of 590 to 613 cm^{-1} and 450 to 462 cm^{-1}, respectively (see Table 3.). The formation of ν_a and ν_b absorption bands revealed the existence of the metal oxide (M-O: Al-O, La-O, Gd-O, Ti-O) stretching vibrations [8, 14]. Besides, the additional bands recorded at 720 to 736 cm^{-1} are also associated with the metal oxide bonds of parent perovskite. During 1057-1069 cm^{-1} and 3072-3617 cm^{-1} wave number range, the peaks are tailored owing to the O-H stretching and bending vibrations of H_2O molecules absorbed by the AGLTO nanoparticles [8, 14]. This implied that all the contents are affected with moisture up to smaller extent.

Table.3. Data on FTIR spectra of AGLTO nanoparticles

y	A-site vibrational frequency υ_a (cm^{-1})	B-site vibrational frequency υ_b (cm^{-1})
0.01	613.4	462.42
0.02	581.8	460.66
0.03	594.08	451.88
0.04	590.57	460.66

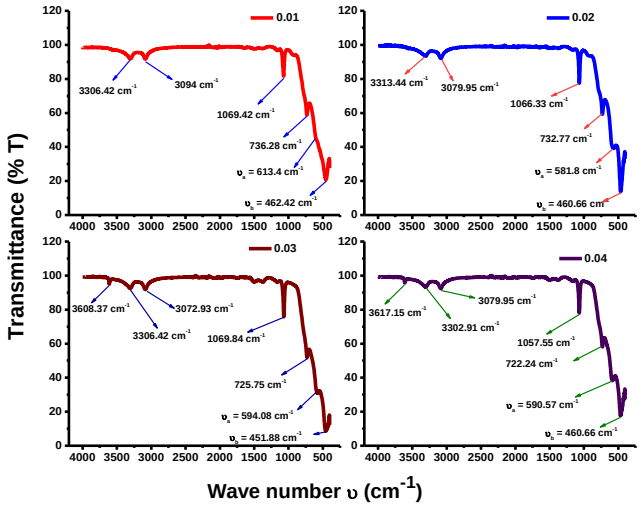

Fig.5. FTIR spectra of AGLTO nanoparticles

6. CONCLUSION

The AGLTO nanoparticles were prepared using the hydrothermal method. The XRD patterns of all samples indicated the highest peak at 13.472°. Also, the average crystallite size (D) was noted to be changing from 23.2 to 41.5 nm for AGLTO samples. The dislocation density (ρ) values are between 5.806 x 10^{14} and 18.57 x 10^{14} m^{-2} respectively; an alternative form of the Gd contents is y = 0.01 to 0.04. The W - H plots based on Scherrer's theory and the values ε' & D' is a good agreement is. Furthermore, the optical band gap (E_g) was found to be increasing from

International Journal of Engineering Research & Technology (IJERT)
ISSN: 2278-0181
Vol. 10 Issue 09, September-2021

3.293 to 3.372 eV as a function of 'y'. The formation of ν_a and ν_b absorption bands revealed the existence of the M-O stretching vibrations.

REFERENCES

[1] Saparjya, S., Behera, S., Badapanda, T. et al., Effects of La^{+3} addition on the phase transition, microstructure, and electrical properties of $Ba_{0.85}Ca_{0.15}Zr_{0.1}Ti_{0.9}O_3$ ceramics. J Mater Sci:Mater Electron (2020). https://doi.org/10.1007/s10854-020-03352-4

[2] Sahu K, Murty VVS, Novel sol-gel method of synthesis of pure and aluminum doped TiO_2 nanoparticles, Indian Journal of Pure & Applied Physics 54 (2016) 485 – 488

[3] Azarniya, A., Azarniya, A., Hosseini, H. R. M., & Simchi, A, Nanostructured aluminium titanate (Al_2TiO_5) particles and nanofibers: Synthesis and mechanism of microstructural evolution. Materials Characterization, 103 (2015) 125–132

[4] Bakhshandeh, F., Azarniya, A., Madaah Hosseini, H. R., & Jafari, S, Are aluminum titanate-based nanostructures new photocatalytic materials? Possibilities and perspectives, Journal of Photochemistry and Photobiology A: Chemistry, 353 (2018) 316 –324

[5] Ewais, E. M. M., Besisa, N. H. A., & Ahmed A, Aluminum titanate based ceramics from aluminum sludge waste. Ceramics International, 43 (2017) 10277 – 10287

[6] Tang, H., He, J., & Persello, J., Giant electrorheological effects of aluminum-doped TiO_2 nanoparticles. Particuology, 8 (2010) 442 – 446

[7] S. Dastagiri, M.V. Lakshmaiah, K.C.B. Naidu, N. Suresh Kumar, A. Khan, Induced dielectric behavior in high dense $Al_xLa_{1-x}TiO_3$ (x = 0.2–0.8) nanospheres, J. Mater. Sci. Mater. Electron 30 (2019) 20253 – 20264

[8] D. Kothandan, R. Jeevan Kumar, M. Prakash, K.Chandra Babu Naidu, Structural, Morphological and Optical Properties of $Ba_{1-x}Cu_xTiO_3$ (X = 0.2, 0.4, 0.6, 0.8) Nanoparticles by Hydrothermal Method, Materials Chemistry and Physics 215 (2018) 310–315

[9] R.D. Shannon Revised Effective Ionic Radii and Systematic Studies of Interatomic Distances in Halides and Chalcogenides, *Acta Cryst.* A 32 (1976) 751-767.

[10] VD Mote, Y Purushotham, and BN Dole, Williamson-Hall analysis in estimation of lattice strain in nanometer-sized zno particles, Journal of Theoretical and applied Physics, 6:6, 2251-7251 (2012).

[11] N. S. Kumar, R. P. Suvarna and K. C. B. Naidu, Sol-Gel Synthesized and Microwave Heated $Pb_{0.8-y}La_yCo_{0.2}TiO_3$ (y= 0.2–0.8) Nanoparticles: Structural, Morphological and Dielectric Properties, Ceramics International 44 (2018) 18189-18199

[12] S. Dastagiri, M. V. Lakshmaiah, K. Chandra Babu Naidu, Defect dipole polarization mechanism in low-dimensional Europium substituted $Al_{0.8}La_{0.2}TiO_3$ nanostructures, Physica E: Low-dimensional Systems and Nanostructures 120 (2020) 114058

[13] N. Raghuram, T. Subba Rao, K. Chandra Babu Naidu, Electrical and impedance spectroscopy properties of hydrothermally synthesized $Ba_{0.2}Sr_{0.8-y}La_yFe_{12}O_{19}$ (y = 0.2 - 0.8) nanorods, Ceramics International 46 (2020) 5894-5906

[14] N. Raghuram, T. S. Rao, K. C. B. Naidu, Investigations on Functional Properties of Hydrothermally Synthesized $Ba_{1-x}Sr_xFe_{12}O_{19}$ (x = 0.0 - 0.8) Nanoparticles, Material Science in Semiconductor Processing 94 (2019) 136-150